Sedimentary Geology 243–244 (2012) 155–168

Contents lists available at SciVerse ScienceDirect

Sedimentary Geology

journal homepage: www.elsevier.com/locate/sedgeo

Formation processes of methane-derived authigenic carbonates from the Gulf of Cadiz

Vitor H. Magalhães [a,*], Luis M. Pinheiro [a], Michael K. Ivanov [b], Elena Kozlova [b], Valentina Blinova [b], J. Kolganova [b], Crisogono Vasconcelos [c], Judith A. McKenzie [c], Stefano M. Bernasconi [c], Achim J. Kopf [d], Victor Díaz-del-Río [e], F. Javier González [f], Luis Somoza [f]

[a] CESAM & Department of Geosciences, University of Aveiro, 3810-193 Aveiro, Portugal
[b] UNESCO Center for Marine Geosciences, Moscow State University, Russia
[c] Geological Institute, ETH-Zurich, CH-8092 Zürich, Switzerland
[d] MARUM - Center for Marine Environmental Sciences, University of Bremen, Germany
[e] Instituto Español de Oceanografia, Fuengirola, 29640 Malaga, Spain
[f] IGME Geological Survey of Spain, Rios Rosas 23, 28003 Madrid, Spain

ARTICLE INFO

Article history:
Received 3 February 2011
Received in revised form 27 October 2011
Accepted 30 October 2011
Available online 10 November 2011

Editor: B. Jones

Keywords:
Methane-derived authigenic carbonates
Dolomite chimneys
Aragonite pavements
Cold-seeps
Anaerobic oxidation of methane
Gulf of Cadiz

ABSTRACT

The Gulf of Cadiz, NE Atlantic, represents an area of extensive formation of methane-derived authigenic carbonates (MDAC), indicative of fluid seepage. These MDAC, that reach extraordinary length and thickness, were geophysically mapped and sampled and the recovered carbonate-cemented material has $\delta^{13}C$ values as low as −56.2‰ VPDB, indicating methane as the major carbon source. The MDAC form two main lithologic groups, one mainly comprising dolomite and the second dominated by aragonite. The dolomite-dominated samples were found along fault-controlled diapiric ridges, on some mud volcanoes and mud diapirs, all on the pathway of the Mediterranean Outflow Water, and along fault scarps. Aragonite pavements were found associated with mud volcanoes and along fault scarps, but are otherwise not restricted to the pathways of the Mediterranean Outflow Water. Based on the results from this study, we propose that the two lithologic groups reflect different geochemical formation environments associated with a formation model based on their morphology, mineralogy and geochemistry. The aragonite-dominated samples represent precipitation of authigenic carbonates at the sediment–seawater interface or close to it, in a high alkalinity environment resulting from anaerobic oxidation of methane-rich fluids venting into sulphate-bearing porewaters. In contrast, the dolomite-dominated samples result from cementation along fluid conduits inside the sedimentary column with a somewhat restricted seawater ventilation. The dolomite chimneys form in places presently swept by the strong flow of the Mediterranean undercurrent so that the unconsolidated sediments are eroded and the chimneys are exposed at the seafloor. The widespread and large abundance of MDAC is a direct evidence of extensive methane seepage episodes in the Gulf of Cadiz. The coincidence of the different lithologic types in close spatial and temporal association indicates a persistence of seepage episodes in some structures over large periods of time.

1. Introduction

Fluid seepage has been recognised as a worldwide widespread phenomenon in different marine settings of both active and passive continental margins, in both the present-day marine environment (Kulm et al., 1986; Hovland et al., 1987; Ritger et al., 1987; Matsumoto, 1990; Paull et al., 1992; Roberts and Aharon, 1994; Greinert et al., 2001; Moore et al., 2004; Meister et al., 2006; Judd and Hovland, 2007; Meister et al., 2007; Campbell et al., 2010) and throughout the geological record (Campbell et al., 2002; Peckmann and Thiel, 2004; Nyman et al., 2010). The precipitation of authigenic carbonates associated with the seepage of methane-rich fluids is the result of the anaerobic methane oxidation coupled with sulphate reduction by consortia of archaea and bacteria (e.g. Kulm et al., 1986; Hovland et al., 1987; Boetius et al., 2000; Greinert et al., 2001). The formation of these methane-derived authigenic carbonates (MDAC) at cold seeps is a common process and depending on the particular geochemical formation conditions different authigenic carbonates (calcite, Mg-calcite, aragonite, proto-dolomite and dolomite) will precipitate (e.g. Burton, 1993; Greinert et al., 2001).

Since 1999, eight research cruises were conducted on board the *R/V Professor Logachev* to investigate the occurrence of mud volcanism, fluid seepage and gas hydrates in the Gulf of Cadiz (Kenyon et al., 2000; Gardner, 2001; Kenyon et al., 2001, 2002, 2003; Pinheiro et al., 2003).

* Corresponding author.
E-mail address: vhm@ua.pt (V.H. Magalhães).

0037-0738/$ – see front matter © 2011 Elsevier B.V. All rights reserved.
doi:10.1016/j.sedgeo.2011.10.013

So far, 42 mud volcanoes (Fig. 1) were confirmed by coring with the recovery of gas (methane with variable amounts of higher homologues) saturated mud breccia. Gas hydrates were recovered from four mud volcanoes but evidences of their presence were identified on several others (Pinheiro et al., 2006). Active fluid venting in the Gulf of Cadiz is indicated by: (1) gas bubbling at the Mercator mud volcano (Akhmetzhanov et al., 2007); (2) mud breccias with methane-rich pore fluids (Stadnitskaia et al., 2001; Niemann et al., 2006; Stadnitskaia et al., 2006; Hensen et al., 2007; Nuzzo et al., 2009); (3) the presence of associated chemosynthetic fauna (Rodrigues and Cunha, 2005); (4) extensive areas of MDAC occurrences (Díaz-del-Río et al., 2003; Magalhães, 2007; Gonzalez et al., 2009); and (5) gas hydrates (Mazurenko et al., 2002; Pinheiro et al., 2003; Nuzzo et al., 2009).

For the present work we used the geophysical data and the extensive number of carbonate samples retrieved during the *R/V Professor Logachev* Training-Through-Research cruises TTR09 (Kenyon et al., 2000), TTR10 (Kenyon et al., 2001), TTR11 (Kenyon et al., 2002), TTR12 (Kenyon et al., 2003), TTR14 (Kenyon et al., 2006), TTR15 (Akhmetzhanov et al., 2007), TTR16 (Akhmetzhanov et al., 2008) and TTR17. This dataset was complemented with data from the *R/V Cornide de Saavedra* Anastasya 2000 and 2001 cruises (Somoza et al., 2002; Díaz-del-Río et al., 2003), and from the 2003 *R/V Sonne* Gibraltar Arc Processes (GAP) cruise (Kopf et al., 2004).

Geophysical data, seafloor video observations and samples retrieved during the research cruises show the presence of large fields, frequently with high density of authigenic carbonates. These high density MDAC occurrences in the Gulf of Cadiz, reported here for the first time, are distributed from the upper continental slope up to depths of 4000 m on the lower continental rise of the Gulf of Cadiz. Such occurrences are not frequently reported in other cold seepage regions and (Fig. 1) are much more extensive and widespread than previously reported by Díaz-del-Río et al. (2003), Gonzalez et al. (2009) and León et al. (2010). We report here, for the first time in this region, the differentiated distribution of the different MDAC lithologies and the geological setting dependency, with dolomite lithologies found only in fluid escape structures of the upper slope of the margin while the aragonite lithologies are found associated with the mud volcanoes over all the margins. These MDAC demonstrate the existence of abundant and intense episodes of methane seepage in the Gulf of Cadiz. The close association of the different types of authigenic carbonates found at some sites of the Gulf of Cadiz, with their high abundance and their distinct characteristics, is rarely reported in the literature. Some of these authigenic carbonate lithologies are here described for the first time in this area.

In this paper, we present, for the first time, a comprehensive overview and the detailed characterisation of all the different types of MDAC from the Gulf of Cadiz, based on the extensive number of collected samples. Here we characterise their mineralogy, geochemistry, and stable C and O isotopic compositions, investigate the relationships between distinct geochemical environments and the resulting authigenic minerals and propose a formation model for the different MDAC lithologies. The proposed model for MDAC formation in the Gulf of Cadiz, considering the different geological settings (mud cones, mud volcanoes, diapiric ridges and faults zones) and the different lithologies, associated with modern or recent cold-seeps, and accounting for the potential involvement of gas hydrate formation/destabilisation in their precipitation, contributes to a better understanding of the particular biogeochemical processes at methane-seeps and provides constraints on the associated fluid venting processes.

2. Geological and oceanographic setting

The Gulf of Cadiz is a sedimentary wedge subjected to tectonically-induced compaction (Gutscher et al., 2002), where extensive mud volcanism and mud diapirism indicate the presence of gas-rich overpressured sediments at depth (Pinheiro et al., 2003; Somoza et al., 2003). Some of the mud volcanoes on the Moroccan margin appear to be located along major NW–SE- and NE–SW-trending faults identifiable on side-scan sonar imagery (Gardner, 2001). In other places, the mud volcanoes appear to be located at the intersection between approximately WNW–SSE to NW–SE and NE–SW strike–slip faults and thrusts of variable orientation related to the formation of the Gibraltar Arc (Pinheiro et al., 2006). The Eurasian–African plate boundary transpressional setting appears to control the formation and trend of the

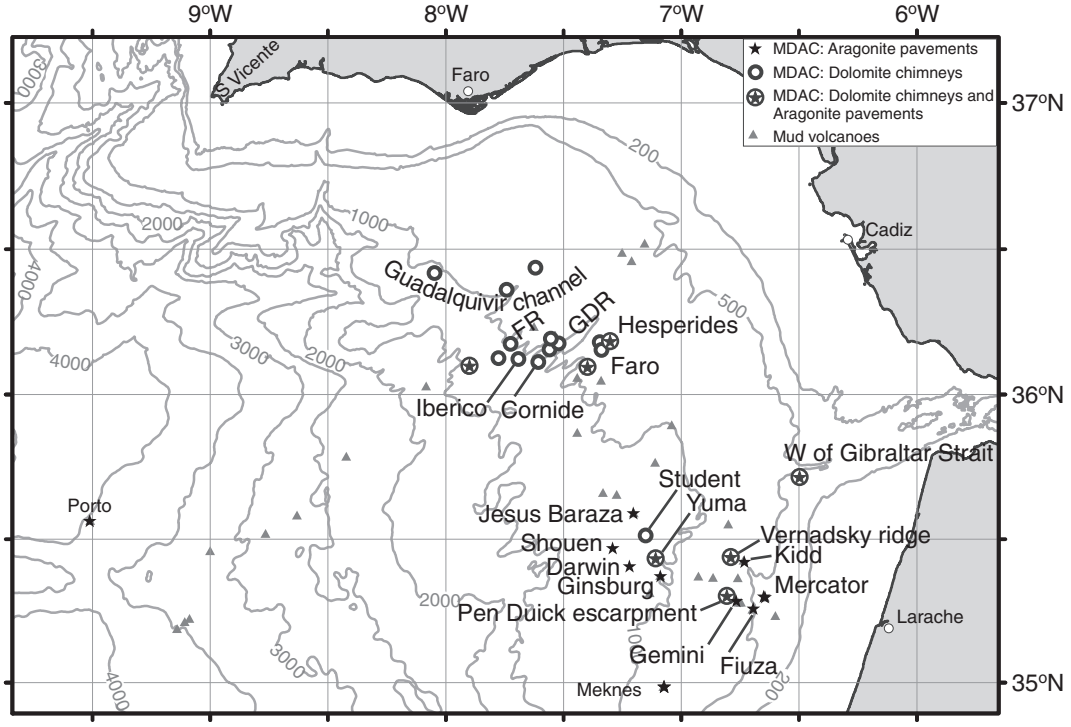

Fig. 1. Map of the Gulf of Cadiz, showing the location of mud volcanoes, mud diapirs and carbonate crusts and chimneys. FR: Formosa Ridge, GDR: Guadalquivir Diapiric Ridge.

diapiric ridges (Guadalquivir Diapiric Ridge and Formosa Ridge) and the salt/shale arched wedges generated by movement of the shale/salt deposits of the olistostrome masses or deeper plastic materials (Medialdea et al., 2004; León et al., 2006; Medialdea et al., 2009; Terrinha et al., 2009).

The MDAC in the Gulf of Cadiz occur at water depths ranging from 400 to 4100 m, in association with mud volcanoes (Faro, Hesperides, Yuma, Ginsburg, Mercator, Adamastor, Meknes, Jesus Baraza, Kidd, Fiuza, Darwin, Shouen and Porto), mud diapirs (Iberico, Cornide), fault scarps (Penn Duick and Vernadsky escarpments), and along fault-controlled diapiric ridges (Guadalquivir Diapiric Ridge and Formosa Ridge). MDAC occurrences are also found along the Guadalquivir and Cadiz Channels, where they cut the Guadalquivir Diapiric Ridge, the Formosa Ridge and on the Mediterranean Outflow Water (MOW) channel, west of the Gibraltar Strait (Fig. 1). The re-examination of samples collected during an earlier (1976) cruise on the northern slope of the Guadalquivir Channel (Gaspar, 1984) also showed the presence of similar authigenic carbonates. The geological setting of the MDAC occurrences and their field relationships with the mud volcanoes, mud diapirs, diapiric ridges or faults, indicate that these structures are preferential sites for dewatering of the sedimentary pile and upward fluid migration. It has also been suggested that some of the widespread shallow fluid venting at the seafloor, particularly in the area of occurrence of MDAC south and southwest of the Guadalquivir Diapiric Ridge and in the Formosa Ridge, might be related to the local destabilisation of gas hydrate-rich sediments, in contact with the MOW (Gardner et al., 2001; Díaz-del-Río et al., 2003; Pinheiro et al., 2003; Magalhães, 2007).

The present day oceanography in the Gulf of Cadiz is dominated by the exchange of water masses between the Atlantic Ocean and the Mediterranean Sea. Highly saline, warm near-bottom MOW flows through the Gibraltar Strait into the Atlantic, while less saline Atlantic water enters the Mediterranean Sea at the surface. Along the northern margin of the Gulf of Cadiz, between 400 and 1200 m water depth, the MOW flows near the seafloor and is affected by the slope morphology, which subdivides it into minor branches, producing meddies (Baringer and Price, 1999; Bower et al., 2002) and affecting the surficial sediments by erosion and deposition of contourite drifts (Hernandez-Molina et al., 2006).

3. Material and methods

The samples used in this study were collected by dredging and by video-controlled grab, and are representative of all the presently known MDAC occurrences in the Gulf of Cadiz (Fig. 1). The characterisation of the morphology and sizes of the authigenic carbonates was based on underwater video observations and the retrieved samples.

The petrography of the carbonates was determined on polished and thin sections by standard petrographic and cathodoluminescence techniques. Scanning electron microscope (SEM) observations were carried out, coupled with energy dispersive spectrometer X-ray elemental analysis (EDS), on fresh fractured surfaces and on samples etched with 1% HCl for 3–4 min. Samples for X-ray diffraction (XRD), $^{87}Sr/^{86}Sr$, total organic carbon, carbonate content, and carbon and oxygen stable isotopes were extracted from transversal and longitudinal cuts of the authigenic carbonates and micro-drilled along orthogonal profiles. The bulk mineralogy was determined by XRD (Table 1) using a Scintag X-ray diffractometer with CuKα radiation (1.5405 Å wavelength). Scans were done from 5° to 60° 2θ at 0.02°/s, using 40 kV accelerating voltage and 30 mA current. Peak identification and relative abundance estimates of minerals were determined using the Scintag interpretation software and the MacDiff® software packages. The Mg:Ca ratio of the carbonate minerals was calculated from the shift of the d-spacing of the (104) reflection peak of calcite and dolomite from their stoichiometric peak positions in the diffraction spectra (Goldsmith and Graf, 1958; Lumsden, 1979).

Samples (100–200 μg) for carbon and oxygen stable isotopic analyses were reacted (10 min) at 90 °C with 100% phosphoric acid on an automated carbonate device connected to a VG-PRISM mass spectrometer calibrated with NBS18, NBS19 and NBS20 standards. The results are reported in the conventional δ ‰-notation with reference to VPDB (Vienna Peedee Belemnite). For the dolomite samples (>20% of dolomite) $\delta^{18}O$ was calculated with the Rosenbaum and Sheppard (1986) fractionation factor. Analytical reproducibility of the method, based on repeated analysis of standards is better than ±0.1‰ for both carbon and oxygen.

Samples for $^{87}Sr/^{86}Sr$ analysis were dissolved in 10 ml, 1.0 N ultrapure acetic acid, centrifuged, and the liquid phase was evaporated to dryness. Then, Sr was separated using a cation-exchange column (AG8 50 W BioRad) with HCl 2.5 N as eluant. After chemical separation, the samples were loaded on a single Ta filament with H_3PO_4 and analysed using a VG-Sector 54 Thermal Ionization Mass Spectrometer at the Central Analysis Lab of the Aveiro University. The analytical reproducibility of the method, based on repeated standards (SRM-987), is better than ±0.0000070.

The carbonate and organic carbon contents were determined using a LECO CHNS-932 elemental analyser. For each sub-sample, three replicates of powdered and homogenised bulk material (2 mg) were analysed. The same set of sub-samples was later subjected to combustion for 8 h through a predefined stepwise increase in temperature up to 400 °C to remove organic carbon, and re-analysed for inorganic carbon. The organic carbon content was determined by the difference between total carbon and inorganic carbon concentration. Results are presented in weight percent (wt.%). The relative precision of repeated standard measurements was 0.03 wt.%.

4. Results

4.1. Morphology, texture and mineralogy of MDAC

Based on their morphology, texture and mineralogy, the authigenic carbonates were classified into two main types: *(i)* dolomite- and high-Mg calcite-dominated crusts, irregular massive forms and chimneys (Fig. 2), and *(ii)* aragonite-dominated crusts or pavements and build-ups (Fig. 3). The dolomite-dominated carbonates were further subdivided into: *(a)* dolomite crusts; *(b)* dolomite chimneys; and *(c)* irregular massive forms (Fig. 2). The aragonite-dominated build-ups or pavements were subdivided into: *(a)* lithified mud volcano breccias; *(b)* lithified pelagic sediments; *(c)* shell crusts; *(d)* intraformational breccias; and *(e)* lithified fragments of dolomite chimneys (Fig. 3).

4.1.1. Dolomite-dominated authigenic carbonates

The dolomite chimneys, crusts and irregular massive forms only differ in their morphology (Figs. 2 and 4A). They all consist of medium to tightly carbonate-cemented mudstones, siltstones and sandstones (Fig. 5A–B) with dolomite, protodolomite, high-Mg calcite, calcite, quartz, feldspar and clays (Table 1). The detrital fraction consists of a fossiliferous matrix with abundant planktonic foraminifera, ostracods, pellets and silty terrigenous grains of quartz, calcite, feldspars, zircon, apatite and clays. Iron and manganese oxy-hydroxides (goethite, manganese oxides, 7 and 10 Å manganates) are responsible for the variable brownish oxidation colour of the samples.

All samples show low porosity with absence of mega-pores and scarce fractures or cracks. The cement is composed of micrite to micro-sparite as equigranular rhombohedric calcite, high-Mg calcite, protodolomite and dolomite crystals of less than 10 μm. The texture varies from isolated rhombohedra to aggregates of interlocking subhedral to euhedral crystals on a tight mosaic (sucrosic texture) of interlocking subhedral crystals. Dissolution or replacing of detrital grains by the carbonate cement minerals is not observed.

Pyrite occurs mostly as sub-idiomorph to idiomorph microcrystals (<3 μm) forming: *(a)* framboids and small aggregates (<100 μm);

Table 1
Mineralogy, carbonate content and stable isotopic composition of the different defined types of MDAC samples collected in the Gulf of Cadiz.

Relative percentages (wt.%)						Mole Mg (%)				$CaCO_3$ (wt.%)	$CaCO_3$ fraction (wt.%)					$\delta^{13}C$ (VPDB)	$\delta^{18}O$ (VPDB)
Arag	Calc	Mg-Calc	ProtDol	Dol	Detrital	Calc	Mg-Calc	ProtDol	Dol		Arag	Calc	Mg-Calc	ProtDol	Dol		
Dolomite crust (N = 8)																	
–	18	33	–	41	33	3	11	–	46	67	–	30	46	–	60	−29.23	3.89
–	(3–60)	(5–77)	–	(9–88)	(9–56)	(1–5)	(10–11)	–	(44–51)	(44–91)	–	(4–78)	(12–89)	–	(11–100)	(−46.88 to −8.42)	(3.08 to 5.47)
–	6	3	–	8	8	6	3	–	8	8	–	6	3	–	8	7	7
Dolomite chimney (N = 101)																	
–	12	10	10	52	34	3	14	32	47	66	–	21	15	13	78	−33.41	4.22
–	(1–93)	(1–64)	(5–32)	(2–92)	(5–74)	(1–8)	(8–27)	(30–35)	(41–49)	(26–95)	–	(2–98)	(1–97)	(6–39)	(2–100)	(−45.55 to −14.70)	(0.81 to 6.77)
–	72	43	6	101	101	70	43	6	101	101	–	72	43	6	101	87	87
Irregular massive forms (N = 4)																	
–	31	–	29	47	27	4	–	37	45	73	–	41	–	52	61	−24.01	5.41
–	(7–75)	–	(29–29)	(11–81)	(13–45)	(2–8)	–	(37–37)	(43–46)	(55–87)	–	(8–87)	–	(52–52)	(13–92)	(−24.01 to −24.01)	(5.41 to 5.41)
–	4	–	1	3	4	4	–	1	3	4	–	4	–	1	3	1	1
Aragonite pavement—lithified mud volcano mud breccia (N = 14)																	
57	10	10	–	4	23	4	18	–	52	77	74	13	12	–	4	−24.29	3.92
(49–66)	(4–20)	(6–13)	–	(4–4)	(12–39)	(1–6)	(14–22)	–	(52–52)	(61–88)	(60–83)	(7–25)	(10–16)	–	(4–4)	(−27.56 to −21.70)	(3.17 to 4.34)
14	14	14	–	1	14	14	14	–	1	14	14	14	14	–	1	12	12
Aragonite pavement—in-situ breccia (N = 4)																	
70	16	19	–	–	10	3	13	–	–	90	78	17	20	–	–	−16.91	4.71
(57–87)	(4–31)	(19–19)	–	–	(6–14)	(2–5)	(13–13)	–	–	(86–94)	(62–96)	(4–36)	(20–20)	–	–	(−19.10 to −14.25)	(4.03 to 5.18)
4	4	1	–	–	4	4	1	–	–	4	4	4	1	–	–	4	4
Aragonite pavement—shell crust (N = 5)																	
57	11	8	–	2	22	2	17	–	46	77	73	15	11	–	2	−42.23	3.42
(41–76)	(10–12)	(4–13)	–	(2–2)	(6–37)	(1–3)	(9–21)	–	(45–46)	(59–94)	(65–82)	(11–20)	(7–18)	–	(1–3)	(−48.13 to −31.28)	(3.06 to 3.74)
5	5	5	–	1	5	4	5	–	2	5	5	5	5	–	2	3	3
Aragonite pavement—stromatolithic fabric (N = 5)																	
80	7	5	–	–	11	3	18	–	–	89	90	7	6	–	–	−44.50	3.99
(73–85)	(4–10)	(5–5)	–	–	(8–18)	(1–6)	(18–18)	–	–	(82–92)	(89–92)	(4–10)	(6–6)	–	–	(−56.16 to −22.64)	(3.82 to 4.27)
5	5	1	–	–	5	5	1	–	–	5	5	5	1	–	–	5	5
Shell/corals/carbonate tube worms casts, attached to the exterior of the samples (N = 6)																	
46	48	77	–	13	11	5	13	–	46	91	49	53	86	–	15	0.09	2.44
(19–91)	(9–96)	(76–77)	–	(13–13)	(4–19)	(2–8)	(13–13)	–	(46–46)	(81–100)	(24–91)	(9–100)	(85–87)	–	(15–15)	(−3.30 to 2.09)	(2.24 to 2.57)
3	5	2	–	1	5	4	2	–	1	6	3	5	2	–	1	4	4
Shells cemented inside the aragonite pavement (N = 3)																	
39	19	8	–	18	18	3	17	–	55	82	49	23	10	–	22	−12.11	3.04
(34–46)	(10–25)	(6–9)	–	(9–26)	(14–26)	(1–4)	(15–18)	–	(54–55)	(74–86)	(40–62)	(14–30)	(7–12)	–	(12–30)	(−18.30 to −8.84)	(2.93 to 3.11)
3	3	2	–	3	3	2	2	–	3	3	3	3	2	–	3	3	3

Notes: N = number of studied samples. – = indicate that the mineral was not detected. Lithologic types defined according to the text. Arag = Aragonite. Calc = Calcite (mol Mg %<8%). Mg-Calc = high Mg-Calcite (8%<mol Mg %<30%). PrtDol = Protodolomite (30%<mol Mg %<40%). Dol = Dolomite (40%<mol Mg %<55%). Detrital = Detrital Fraction (Quartz, feldspar, clays and other minerals that compose the detrital fraction).
The $\delta^{13}C$ and $\delta^{18}O$ Stable isotopic values are reported in the conventional δ ‰-notation with reference to VPDB. For the dolomite-type samples (>20% of dolomite), $\delta^{18}O$ values are corrected for the analytical offset of +1.63‰, consequence of the unequal oxygen fractionation during the reaction to CO_2.

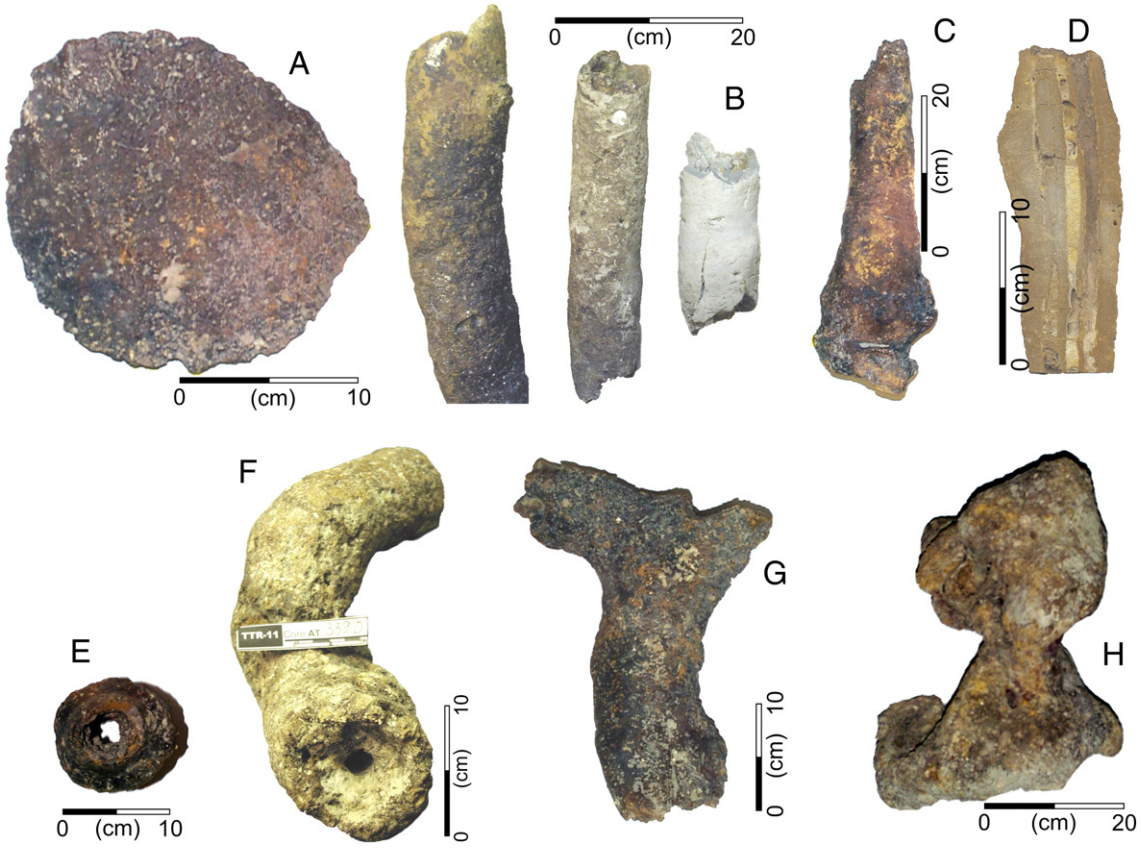

Fig. 2. Illustration of the different morphologic types of dolomite carbonate samples recovered. A: dolomite crust; B–G: dolomite chimneys; B: tubular shape; C: conical shape; D: with two parallel vent channels; E: doughnut shape; F: spiral shape; G: branched shape; H: irregular massive form.

(b) filling intra-clast porosity, as pseudomorphs of bioclasts; *(c)* disseminated in the carbonate matrix; or *(d)* filling cracks and burrows. Organic matter, around and within pyrite micro-crystal aggregates, forming peloidal and clotted microfabrics, is frequently observed and it is interpreted as indicating a microbial origin (e.g., Reitner et al., 1995). Brownish oxidation rims and Fe–Mn oxy-hydroxide

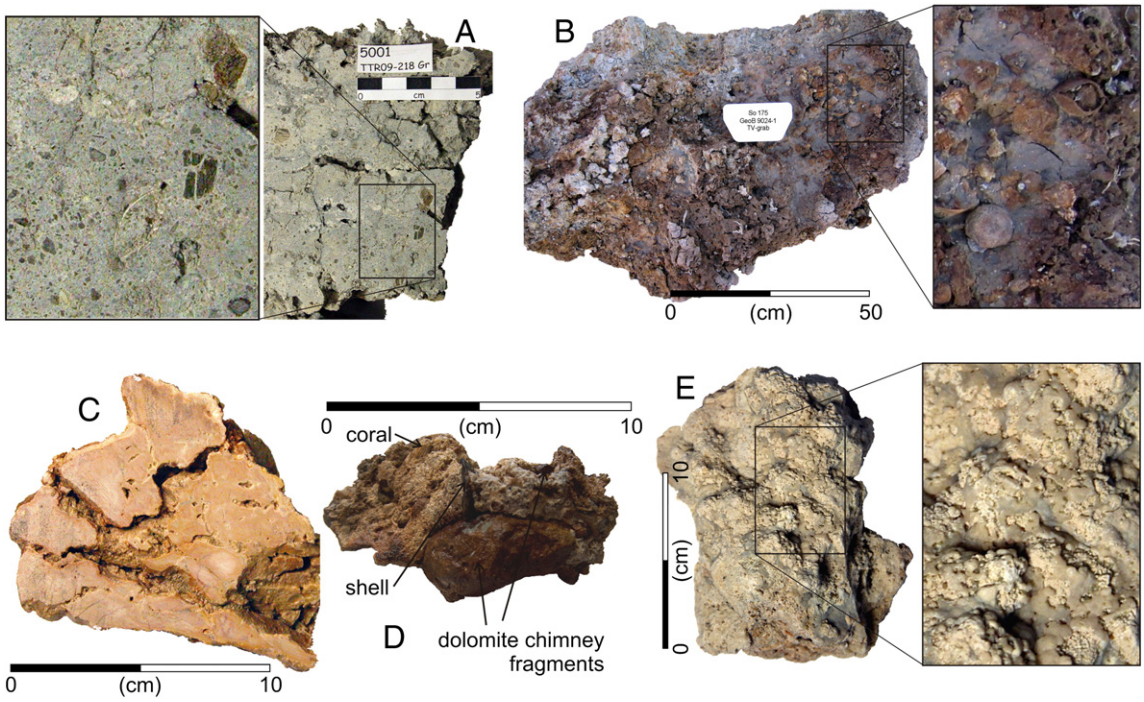

Fig. 3. Illustration of the different aragonite pavement types. A: lithified mud volcano mud breccias; B: shell crusts; C: intraformational breccias; D: lithified clasts of dolomite chimneys and crust fragments; E: stromatolitic layers.

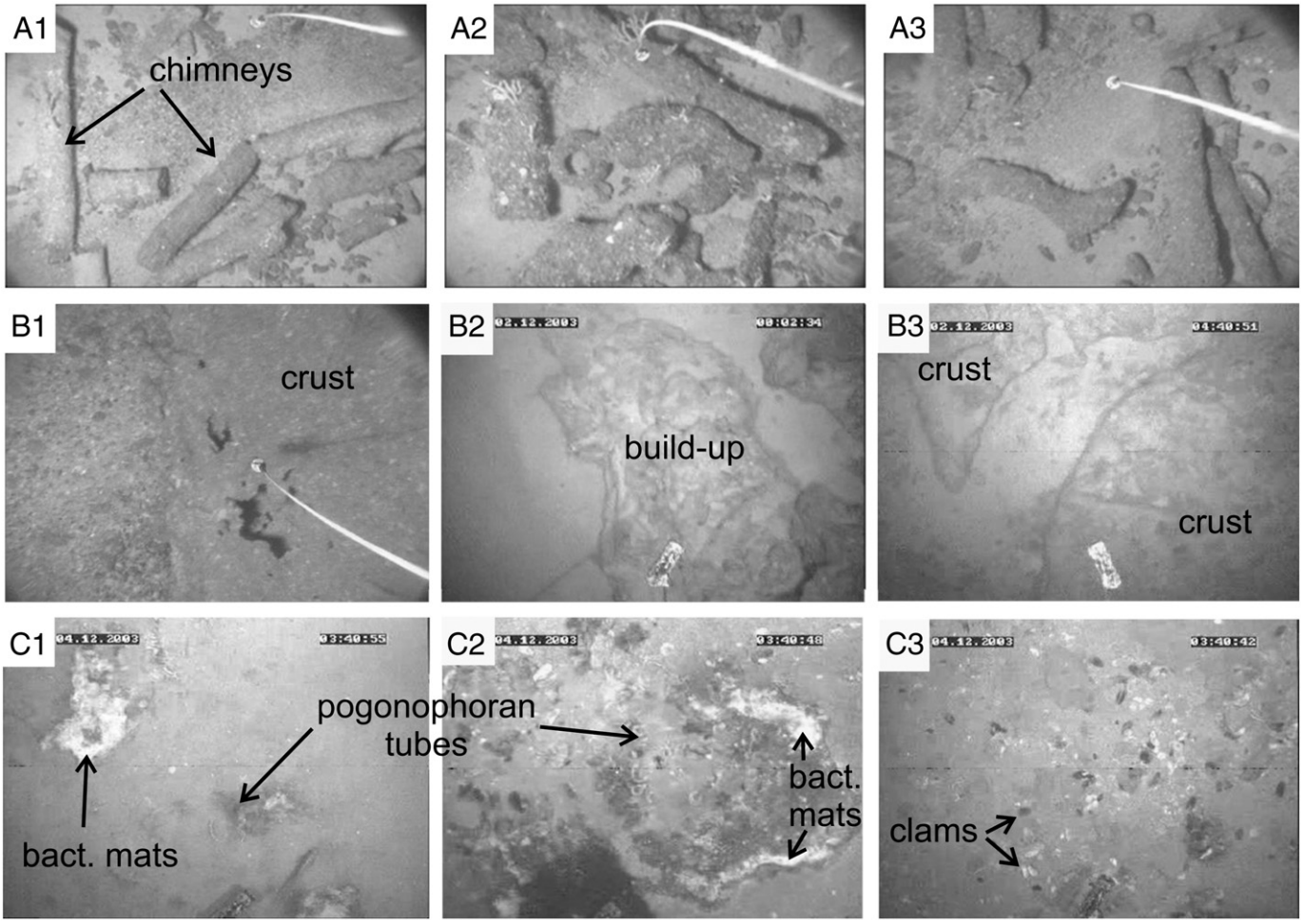

Fig. 4. Bottom photographs taken from the *R/V Professor Logachev* underwater video camera from video profiles (cruises: TTR11, 12 and 14). A1–3: dolomite chimneys from the Iberico mud cone, on the MOW channel and on the Formosa Ridge. B1–3: aragonite pavements on the Faro and Hesperides mud volcanoes. C1–3: chemosynthetic fauna associated with aragonite pavement occurrences on the Faro mud volcano. The field of view of the pictures is approximately 2.5 m across.

pseudomorphs after pyrite are frequently observed in samples affected by intense oxidation. In some samples, heterogeneous massive pyrite cements the pore-space in between sub-idiomorphic to idiomorphic dolomite and possibly Fe-dolomite crystals.

During visible-light petrography, cathodoluminescence, and SEM studies, prominent zonation of the dolomite crystals was not observed. Also, no textural evidence of calcite replacement by dolomite was found, possibly indicating the primary origin of dolomite. Cathodoluminescence microscopy and SEM observations indicate the absence of significant amounts of Fe or Mn in the carbonate phases. Estimates of the Mg/Ca ratios are reported in Table 1, based on the shift of the d(104) peak, with a maximum error of 9 mol $MgCO_3$% (Goldsmith and Graf, 1958). The dolomite shows $MgCO_3$ contents between 45 and 47 mol% (Table 1). Pelagic sediments collected in the vicinity of the MDAC fields contain no dolomite, and only minor amounts of authigenic dolomite were identified by SEM in the mud breccia matrix from some mud volcanoes (Martin-Puertas et al., 2007), supporting the authigenic origin of the dolomite.

SEM observations allowed the identification of a high diversity of microbially induced fabrics such as: *(1)* microbial filaments; *(2)* high-Mg calcite and dolomite crystal aggregates that mimic microbial filaments through calcification; *(3)* carbonate rods with brush-like terminations (Magalhães, 2007). Carbonates with dumbbell-like and cauliflower structures, while not exclusive indicators of a microbial origin, were also observed (Magalhães, 2007). Similar textures have been observed in carbonates from laboratory experiments using sulphate-reducing bacteria (Vasconcelos et al., 1995; Gournay et al., 1999; Van Lith et al., 2003). These microbial filaments and structures match the typical size of the microbial filaments and structures and therefore indicate a microbial activity involvement in the precipitation of the authigenic carbonates. These observations are also supported by archaea-diagnostic AOM biomarkers identified on some dolomite chimneys (Magalhães, 2007).

4.1.1.1. Dolomite chimneys. The terminology dolomite "chimney" is used here in a descriptive sense, indicating samples with a pipe-like or a conduit-like morphology without implying a formation in the water column. This terminology is used because it has commonly been used to describe such structures not only in the Gulf of Cadiz (Somoza et al., 2002; Díaz-del-Río et al., 2003), but also in many other cold-seep areas (Kulm and Suess, 1990; Orpin, 1997; Greinert et al., 2001).

The collected chimneys have cylindrical or conical shapes, are 10 to 90 cm long and 1 to 35 cm in diameter. During underwater video observations chimneys up to 4 m long and with diameters up to 0.5 m were identified. Based on the chimney morphologies, several sub-types were defined: *(1)* tubular (single or with 2 or 3 parallel tubes cemented together), *(2)* conical, *(3)* doughnut shaped, *(4)* spiral, and *(5)* branched (Fig. 2). Some chimneys are completely filled, while others have an open vent channel. The filled chimneys commonly exhibit concentric growth ring layers. The external surface of most of the chimneys is iron oxide stained, with a dark red to dark brown colour, whereas the non-oxidised chimneys are pale yellow to medium light grey colour (Fig. 2).

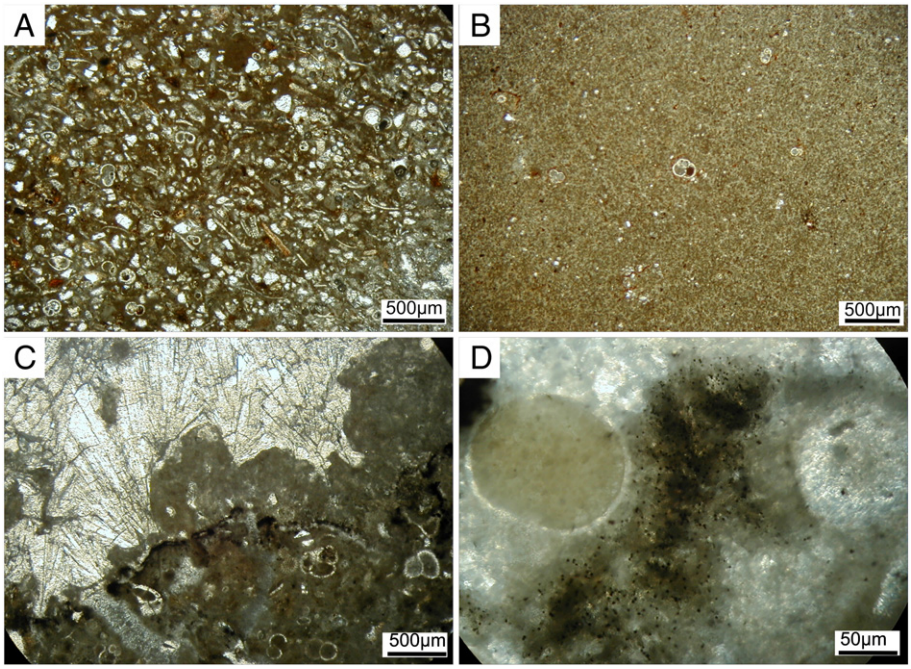

Fig. 5. Thin sections of dolomite crusts and chimneys (A–B). Sandstone (A) and wackestone (B), where it is possible to recognise that the detrital fraction of bioclasts and terrigenous grains is cemented by a micrite to micro-spar carbonate cement with peloidal and clotted microfabric. Thin sections of aragonite pavements (C–D). C: two carbonate cement phases, the clotted micrite or microbial pelmicrite cement (at the lower-right half of the field of view), and a later cementation stage by acicular (almost pure) aragonite that fills the pore spaces, fractures and open cracks (the upper-left half of the field of view). D: detail of the peloidal and clotted microfabrics. All microphotographs are in plane-polarized light.

Colonisation of the chimneys by benthic fauna is common, both living and dead specimens, including encrusting sponges, cold-water corals, bivalves or brachiopod clusters, especially on chimneys with a dark iron oxide coating. These samples frequently show scavenger burrows of 1 to 2 mm in diameter and 1–3 cm in length (most probably burrowing barnacles or gastropods, serpulid worms and encrusting sponges). No mollusc shells or fragments of heterotrophic organisms were found cemented in the chimneys. This contrasts with what is observed in the aragonite pavement samples (Section 4.1.2) and described elsewhere for sites of active seepage (e.g., Paull et al., 1992; Sibuet and Olu, 1998).

Some of the chimneys show incipient layering perpendicular to the axis of the vent conduit, which occasionally leads to the segmentation and fragmentation of the chimneys. When this segmentation is closely spaced, the chimneys form doughnut-shape fragments. In other chimneys, the layering is revealed by a coarser grain size of the detrital fraction, sometimes associated with nodular protuberances or irregular massive forms that locally increase the diameter of the chimney. These are interpreted as zones of enhanced cementation of higher permeability sediment layers. In one sample, it was observed that a dolomite crust was being formed perpendicular to the chimney, as the result of cementation along a more permeable layer perpendicular to the conduit.

4.1.1.2. Dolomite crusts. The only distinctive characteristic of the dolomite crusts in relation to the dolomite chimneys and the irregular massive forms is their morphology. Dolomite crusts have planar shapes, up to 10 cm thick and up to 70 cm across (Fig. 2A). It has to be noted that, in contrast to the aragonite pavements, dolomite crusts show no internal structure, a low porosity, no macroporosity or internal channels and neither shells nor biogenic components (except for foraminifera and coccoliths).

4.1.1.3. Irregular massive forms. This type corresponds to nodular, massive, round or irregular forms (Fig. 2H), with sizes up to 45 cm. The texture, colour, petrography and mineralogy (Table 1) of these samples are similar to those of the dolomite chimneys and crusts.

4.1.2. Aragonite-dominated authigenic carbonates

Aragonite-dominated authigenic carbonates form crusts and pavements or irregular blocky build-ups at the seafloor. Different lithologic types were identified: *(i)* lithified mud volcano breccias; *(ii)* lithified pelagic sediments; *(iii)* shell crusts; *(iv)* intraformational breccias; and *(v)* lithified fragments of dolomite chimneys/crusts. Several of these sub-types can coexist at the same location and sometimes in the same sample. These sub-types have common petrographic and mineralogical characteristics.

All the aragonite crusts, pavements and build-ups are whitish or light brownish grey to dark grey. Authigenic aragonite is the dominant mineral with subordinate authigenic calcite and high-Mg calcite (Table 1), cementing a detrital fraction of quartz, feldspars, clays, mud volcano mud breccia clasts, shell fragments, foraminifera and calcareous nannofossils. The aragonite-dominated carbonates have only a small percentage (<4 wt.%) or, most frequently, no dolomite, with a significant macro-porosity (voids, fractures, tubular and irregular cavities some of them interconnected) and high percentages of open inter-granular pore space, indicating formation within very weakly compacted sediments (Fig. 3). SEM observations revealed microbial filaments, microbial and mucosic biofilm sheets and threads draped between aragonite needles, aragonite batons, ball-capped batons (0.20–0.70 μm) and nannograins, similar to described bacterially-induced fabrics elsewhere (Buczynski and Chafetz, 1991; Van Lith et al., 2003). These observations are also supported by archaea-diagnostic AOM biomarkers and sulphate-reducers bacteria biomarkers identified on aragonite-dominated pavements (Magalhães, 2007).

Two distinct texture types of the authigenic cements can be defined in the aragonite pavements and build-ups: fine-grained texture and stromatolitic fibrous texture (Fig. 5C). The fine-grained granular texture is characterised by micrite to microspar granular and fibrous aragonite, calcite and Mg-calcite crystals. Pyrite is found dispersed in the cement as individual spheres and framboids (<100 μm), or as clusters, sometimes forming incipient layers or lineaments (up to 2 cm long). In general, the pyrite is partially oxidised to iron oxides and/or hydroxides. The stromatolitic fibrous texture is present in all

aragonite-dominated samples. It corresponds to parallel laminae, or radiating aggregates and bundles of fibrous aragonite, that cover the internal surfaces of mega pore-spaces, voids, tubular cavities and fractures (Fig. 3E). The fibrous texture always grows over the fine-grained granular texture, and thus represents a later stage of authigenic carbonate formation (Fig. 5C). The stromatolitic layers are up to 10 mm thick and present an external smooth surface with domal, isopachous layers of aggregates and botryoidal rims of fibrous aragonite needles that grow towards the centres of the cavities. The undulating laminated pattern, similar to the cauliflower-like structures of stromatolites, is present on top of and parallel to the cavity surfaces (Fig. 5C–D). Pyrite is found, in general, as framboids or small clusters aligned parallel to the stromatolitic layers, partially to almost completely oxidised.

4.1.2.1. Lithified mud volcano breccias. This aragonite pavement type consists of a very porous, weak to moderately carbonate-cemented mud volcano breccias (Fig. 3A). The lithified mud volcano breccias show irregular block shapes, up to 50 cm across, most probably resulting from the fragmentation, during sampling, of larger pavements that cover the seafloor for several square meters, as observed by underwater video (Fig. 4B). The lithified mud volcano breccias are generally brownish to dark grey or black, indicating a variable reducing environment. Frequently, the upper side of the samples is brownish, corresponding to exposure to oxic seawater, while the lower surface has a dark grey colour corresponding to an anoxic subsurface. Frequent tubular holes, 2 to 8 mm in diameter, are interpreted as Pogonophorid worm tube casts, serving as venting conduits along which fluid migration is focused and around which carbonate precipitation is enhanced. Live Pogonophora and other chemoautotrophic organisms were retrieved together with some of the lithified mud volcano breccias from sites of interpreted more intense or recent venting activity.

4.1.2.2. Lithified pelagic sediments. In this lithology fine-grained clastic sediments (silt to sand-sized quartz and feldspar grains, coccoliths, radiolarians, diatoms and foraminifera skeletons, as well as detrital clay minerals) are cemented forming crusts, pavements and blocks or small mounds of moderately to very strongly cemented carbonates. They usually correspond to large retrieved samples (up to 1 m long and 40 cm thick). Like the lithified mud volcano breccias the lithified pelagic sediments show abundant macroporosity of irregularly shaped and randomly interconnected open cracks and cavities, up to 2 cm wide. Some crusts also exhibit a sharp contrast between the upper surface of the crust, with an intense iron oxide coating indicating exposition to the oxic seawater, and the lower surface with no signs of oxidation, which was in contact with anoxic sediments.

4.1.2.3. Shell crusts. Shell crusts (Fig. 3B) correspond to clusters of bioclasts of *Calyptogena*, *Acharax* (sometimes still enclosed by an intact periostracum indicating in situ cementation), *Pogonophora* and *Vestimentifera* tube worms within lithified mud volcano mud breccias or within lithified pelagic sediment pavements. The incorporation of such high densities of organisms and their characteristics indicate that the crust formation took place near or at the seafloor. Sessile organisms, like small corals, brachiopods and small sponges are also found attached to, and are occasionally incorporated into the crusts.

4.1.2.4. Intraformational breccias. Intraformational breccias (Fig. 3C) are composed of chaotically oriented matrix-like carbonate intraclasts (up to 3 cm in size, interpreted as fragments from previous aragonite pavements), bioturbation casts and shells, and poorly lithified mud breccia clasts of lithified mud volcano breccias. The cement is composed of randomly oriented fibrous sparitic aragonite and/or fine-grained granular poly-phase micrite to microspar aragonite, calcite and high-Mg calcite (the latter, more abundant in the intraclasts). They present medium to high porosity with abundant irregular shaped and randomly interconnected macropores (>100 μm), open cracks and cavities (of cm sizes), that produce the pseudobrecciated collapse texture characteristic of this lithologic type. It is therefore interpreted as a syn-formational breccia, i.e. the fractures and pore spaces were formed and were maintained open during the cementation. Frequently the macropores, open cracks and cavities are covered with stromatolitic layers of botryoidal white aragonite cement. Some of the recovered samples exhibit dissolution surfaces, subsequently covered by later phases of cementation.

4.1.2.5. Lithified fragments of dolomite chimneys/crusts. The lithified fragments of dolomite chimneys/crusts (Fig. 3D) were collected by dredging the flank of the Guadalquivir Channel. They consist of clast-supported breccias, where the clasts are fragments, strongly stained with iron oxides, up to 12 cm in size, with a sub-rounded morphology, indicating a significant transport by deep currents along the steep flank of the channel. These clasts have the petrographic, mineralogical and isotopic characteristics of the dolomite irregular massive forms, crusts and chimneys, and are therefore interpreted as fragments of dolomite chimneys and crusts that got cemented during secondary episodes of MDAC precipitation by the typical aragonite-dominated carbonate cement of porous micrite to microspar granular and fibrous aragonite, calcite and Mg-calcite. The cement has pale to light brown colours indicating variable degrees of oxidation.

4.2. Occurrence and underwater observations

4.2.1. Dolomite crusts and chimneys

Dolomite chimneys, crusts and irregular massive forms occur often very fragmented, and lying on the seafloor, forming high density fields that can have hundreds of meters of extensions (Fig. 4A) located at water depths ranging from 390 m up to 1420 m (Fig. 1). It is rare to find chimneys in a vertical position, protruding from the sediments. In situ and not completely exposed chimneys were only observed along the Cadiz MOW Channel. Some of those chimneys exhibited a sub-parallel orientation relative to the sedimentary layering while others clearly presented a sub-vertical orientation (as is also supported by the apparent layering interpreted in some chimneys). The seafloor occurrences of the dolomite crusts, chimneys and irregular massive forms (Fig. 1) are restricted to areas characterised by moderate to strong bottom currents. These are considered to be able to produce active erosion of the surrounding unconsolidated sediments within which the chimneys grew, inducing the exhumation of the chimneys, which once exposed fall over on the seafloor.

Large colonies of Cnidaria (Hydrozoa and Anthozoa), Mollusca (Gastropoda and Bivalvia), Annelida (Polychaeta), Arthropoda (Decapoda), Brachiopoda, Echinodermata (Crinoidea, Asteroidea, Ophiuroidea, Echinoidea and Holothuroidea) use the carbonates as hard substrates for attachment or inhabitation. Unambiguous chemosynthetic communities were not identified at sites of exclusive occurrence of dolomite chimneys, crusts and irregular massive forms. Chemosynthetic communities were identified only at sites characterised by the occurrence of aragonite pavements. On the Hesperides, Faro and Student mud volcanoes, and in the MOW channel off the Strait of Gibraltar, dolomite chimneys and aragonite pavements were found in close spatial proximity or formed in close association. However, the observed occurrence of the dolomite chimneys as broken and fragmented lying at the seafloor (Fig. 4A), when compared with the in situ occurrence of the aragonite pavements, associated with chemosynthetic organisms (Fig. 4B) and incorporating fragments (frequently sub-rounded) of dolomite chimneys (Fig. 3D) indicate that the two MDAC types were formed during distinct formation periods.

4.2.2. Aragonite crusts, pavements and build-ups

The aragonite pavements appear on the seafloor as build-ups or small mounds, occasionally with dimensions up to 3–4 m; or as rough hard grounds (up to 50–80 cm thick) that can pave the seafloor for areas of several square metres, with a thin or absent sediment cover (Fig. 4B) and their occurrences range from water depths from 350 m up to 4000 m (Fig. 1). Colonisation of these pavements by benthic fauna is frequent. Aggregates of bivalves, most apparently dead, and live chemosynthetic fauna (*Frenulate Siboglinid* tube worms) were identified and sampled at several of the sites where the aragonite pavements occur. Small patches of probable bacterial mats were identified only at one location in the Faro mud volcano (Fig. 4C). They were not detected at the scales normally found in areas of intense and active seepage, like in the Gulf of Mexico (Paull et al., 1985; Roberts and Aharon, 1994) or in the Eastern Mediterranean (Sibuet and Olu, 1998; Olu-Le Roy et al., 2004). The scarcity of chemosynthetic fauna is interpreted as indicating a global present day state of low fluid venting intensity at the seafloor, with only small and rare sites of intermediate fluid venting intensity. This is also confirmed by the low to mid range microbial methane turnover and anaerobic oxidation of methane (AOM) activity measured in some of the Gulf of Cadiz mud volcanoes (Niemann et al., 2006). Only at two sites in the Mercator mud volcano crater, in areas of highly gas-saturated mud breccias, active fluid escape was identified by the observation of gas bubbles escaping from the seafloor.

4.3. $CaCO_3$ and total organic carbon

The carbonate content of the dolomite-dominated MDAC, with a mean value of 72 wt.%, is significantly higher than the mean $CaCO_3$ value of the background sediments (~34 wt.%, Table 1). Therefore, the dolomite-dominated MDAC contain, on average, ~38 wt.% of authigenic carbonate cement (maximum value of 60 wt.%). The carbonate content of the different aragonite crusts and pavements has average values ranging from 77 to 90 wt.% (Table 1), which are significantly higher than the average $CaCO_3$ values of the background sediments (~30 wt.%), indicating that the aragonite crusts and pavements contain 40 to 60 wt.% of authigenic carbonate cement.

The organic carbon contents of the MDAC samples are less than 0.4% (dry wt.%), with an average value of about 0.1%. These values are lower than those characteristic of the pelagic sediments of the slope and rise of the Gulf of Cadiz, which are generally in the range of 0.5% and 1.5% (UGM-LNEG MarSed samples database). The mud volcano mud breccias have organic carbon values between 0.1 and 1.0% (dry wt.%). This may indicate that during the MDAC formation, part of the organic carbon available in the sediments was consumed and reflect the dilution effect by the cement precipitation.

4.4. C and O stable isotopes

The carbon and oxygen stable isotopic compositions and the mineralogy were analysed for 129 bulk MDAC samples and for bivalve shells, corals, and worm tubes sampled from the MDAC samples (Table 1 and Fig. 6). The origin of the MDAC from oxidised methane is supported by their highly negative carbon isotope signature (Fig. 6 and Table 1) ranging from −56.2 to −8.4‰ VPDB. Oxygen isotope values range from 0.8 to 6.8‰ VPDB. No significant differences in the carbon and oxygen isotope values among the different MDAC types are evident (Fig. 6).

The carbon and oxygen isotope ratios of the dolomite chimneys show a regular pattern in some samples. Along radial profiles across the chimneys, the carbon isotope ratios become, in general, heavy towards the periphery while the oxygen isotope ratios become lighter. Large chimneys have, in general, lighter carbon isotope ratios than thinner chimneys (Magalhães, 2007).

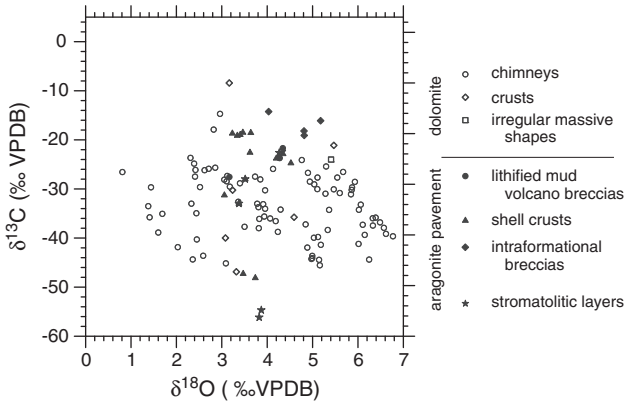

Fig. 6. Isotopic composition of the different authigenic carbonate types, all with negative carbon isotopic values typical of a methane-derived carbon source, and positive oxygen isotopic values.

Shells collected from the aragonite shell crusts have depleted $\delta^{13}C$ values (−12.1‰ VPDB) and slightly enriched $\delta^{18}O$ values (3.0‰ VPDB), while samples of biogenic carbonates (corals and bivalve shells) attached to the surfaces of dolomite chimneys have close to normal seawater isotopic compositions ($\delta^{13}C$ average value of 0.1‰ VPDB and $\delta^{18}O$ average value of 2.4‰ VPDB).

4.5. Sr isotopes and seawater influence

The $^{87}Sr/^{86}Sr$ ratios for the different types of carbonate samples (dolomite chimneys and crusts, and aragonite pavements) show values between 0.709110 and 0.709191 (Table 2). These $^{87}Sr/^{86}Sr$ ratios cluster around the present day seawater value of 0.709175 (Paytan et al., 1993). Thus, the $^{87}Sr/^{86}Sr$ ratios of authigenic carbonates indicate formation from fluids with Sr values similar to those of present day seawater and do not indicate any evident addition of Sr from deep-seated fluids.

5. Discussion

5.1. Estimation of fluid composition and evolution

The carbon isotopic composition of the authigenic carbonates (Fig. 6 and Table 1) is typical of carbonates formed at methane seeps (e.g. Kulm et al., 1986; Hovland et al., 1987; Ritger et al., 1987; Kulm and Suess, 1990; Aharon et al., 1992; Paull et al., 1992; Bohrmann et al., 1998; Greinert et al., 2001; Peckmann et al., 2001; Wiedicke and Weiss, 2006; Kinnaman et al., 2007) and indicates precipitation from oxidation of a moderate to extremely ^{13}C-depleted reservoir. The inference of the composition of the carbon reservoir from the carbonate mineral isotopic composition is complex, because the isotope value mineral composition may reflect mixing from different carbon sources (sediment organic matter, methane, other hydrocarbons, seawater dissolved carbon and marine biogenic carbonate), and furthermore because the fractionation of the carbon will also depend on the extent to which the different carbon

Table 2
Strontium isotope values of MDAC samples.

Sample	MDAC type	$^{87}Sr/^{86}Sr$	Error (2δ)
3458-A3	Dolomite crust (DCr)	0.709191	±0.000060
3463-A8c	Dolomite chimney (DChy)	0.709110	±0.000054
3611-A1	Aragonite pavement (SCr)	0.709183	±0.000054

reservoirs are oxidised. The total organic carbon content of pelagic sediments collected at or near the sites where the MDAC were recovered shows values (up to 0.9%) typical of this area of low to medium primary productivity (Schonfeld, 2001). Therefore, the contribution from in situ diagenetic turnover of organic matter to the porewater total carbon pool from which the MDAC were formed is not expected to be large. In relation to methane and other hydrocarbons as the source for the carbonate carbon, thermogenesis and biogenesis are the most likely potential sources to be considered in the Gulf of Cadiz. The gas-saturated mud breccia from several mud volcanoes shows a mixture of biogenic and thermogenic origins for the hydrocarbon gases, indicating distinctive fluid-generating environments and different secondary processes during fluid transport (Blinova et al., 2006; Stadnitskaia et al., 2006; Hensen et al., 2007). Studies of gas hydrates from mud volcanoes along the Moroccan margin indicate hydrocarbons with high C_2–C_6 (up to 19%) content, also indicating a thermogenic origin for the fluids (Mazurenko et al., 2002). Another potential source for the carbonate carbon is the dissolved carbon from normal seawater and HCO_3^- derived from dissolution of carbonate tests (both with $\delta^{13}C$ values of ~0‰ VPDB). The isotope effect of the dissolved carbon from normal seawater is probably less important compared to the extreme values and high amounts of dissolved carbon resulting from AOM. The strontium isotope values indicate a seawater origin, as strontium is not affected by AOM, it is to be expected that the seawater is also a source for the carbon.

Since many samples have $\delta^{13}C$ values heavier than typical biogenic methane values, mixing with other carbon sources is apparently common. The average $\delta^{13}C$ values of the authigenic carbonates are very close to the average values of the gas hydrates and porewater gases from the mud volcanoes, which indicates a mixture of biogenic and thermogenic gases. As such, the isotopic composition of the authigenic carbonates (Fig. 6) is interpreted as reflecting the mixing of different proportions of thermogenic and biogenic methane-rich fluids with non-methane carbon sources, where seawater is likely the most important.

The oxygen isotope composition of the authigenic carbonates is controlled by a combination of factors, including the carbonate mineralogy and chemistry, the temperature of precipitation and the pore-fluid isotopic composition. The initial pore-fluid composition from which the different carbonate minerals precipitated was reconstructed assuming a temperature of formation ranging between 4 and 14 °C. Regional palaeoceanographic reconstructions (Voelker et al., 2006) point to 4 °C as the minimum seabottom water temperature possible to occur during glacial periods at the sites where the MDAC occur. The upper temperature limit of 14 °C corresponds to the highest measured seabottom water temperature at the shallower sites beneath the MOW (Ambar et al., 2002, CANIGO CTD database). The MDAC samples, as seen in Fig. 6, have bulk isotopic values ranging from 0.8 to 6.8‰ VPDB. The aragonite MDAC samples with heavier isotopic compositions, up to 5.9‰ VPDB, must have been formed from pore water fluids with a minimum isotopic composition of 2.2‰ VSMOW, assuming the (Bohm et al., 2000) fractionation equation and the minimum assumed temperature of formation (4 °C). The estimated calcite isotopic compositions have values up to 5.0‰ VPDB, and must have been formed from pore water fluids with isotopic compositions ranging from 2.8.0 up to 5.1‰ VSMOW, assuming the (Kim and O'Neil, 1997) fractionation equation for the assumed (4–14 °C) temperature range. The estimated dolomite isotopic compositions have values up to 7.4‰ VPDB, must have been formed from pore water fluids with isotopic compositions ranging from 2.0 up to 4.4‰ VSMOW, assuming the (Vasconcelos et al., 2005) fractionation equation and the assumed (4–14 °C) temperature range. The MDAC samples enriched in ^{18}O are therefore interpreted as having precipitated from ^{18}O-rich fluids (more than +2‰ and up to +4‰ SMOW), which were possibly derived from dissociation of gas hydrates (Magalhães, 2007).

5.2. Carbonate mineralogy and geochemical environments

Syn-genetic pyrite within the authigenic carbonate cements implies anaerobic oxidation of methane (AOM) via sulphate reduction (SR). Therefore it is proposed that, during upward fluid migration, methane was anaerobically oxidised in the Sulphate Reduction Zone (SRZ) according to the microbially mediated (Boetius et al., 2000) net chemical reaction (Reeburgh, 1980):

$$CH_4 + SO_4^{2-} \rightarrow HCO_3^- + HS^- + H_2O. \quad (1)$$

As AOM increases the alkalinity of the pore fluids, isotopically light methane carbon is converted to bicarbonate, inducing the precipitation of authigenic carbonates with light carbon isotope ratios (Ritger et al., 1987; Paull et al., 1992). Sulphide, another product of AOM-SR coupling, will be precipitated as pyrite in the presence of Fe^{2+}, remain dissolved or will be consumed by sulphide-based organisms such as *Siboglinum* sp., *Polybrachia* and *Oligograchia* (pogonophora), *Acharax* sp. (solemydae) and *Lucinoma* (Lucinidae) that were collected at the sites where aragonite pavements appeared to be actively forming (Rodrigues and Cunha, 2005). Shallow depths (20 cm below the seafloor) of the sulphate–methane transition zone (SMTZ) were found at active mud volcanoes and at some sites from which MDAC were collected (Niemann et al., 2006; Hensen et al., 2007), indicating that intense upward migration of methane (as gas or fluid) moves the SRZ near to, or even to the seafloor in the case of intense fluxes.

The mineralogy of the authigenic carbonates and their isotopic signature is influenced by the concentration of the cations Ca^{2+}, Mg^{2+}, Fe^{2+} and Mn^{2+}, the complex-forming anions PO_4^{3-} and SO_4^{2-} (considered the most important at this environment as it is the one that is constrained), according to Eq. (1), and temperature (Burton, 1993; Morse et al., 1997). Hence, the different carbonate minerals record distinct formation environments.

5.2.1. Dolomite

Magnesium in seawater that is supersaturated for dolomite precipitation forms the ion-complex $MgSO_4^0$, even at very low SO_4^{2-} concentrations (Baker and Kastner, 1981). Therefore, SO_4^{2-} is an effective inhibitor for dolomite precipitation, even at concentrations less than 5% of its value in seawater. At methane seeps, where there is an efficient system of migration of sulphate-deficient and methane-enriched deep fluids, the SMTZ will be pulled upwards and, according to Eq. (1), AOM-SR contributes to higher HCO_3^- super-saturation and the seawater sulphate will be consumed. As a result, the amount of $MgSO_4^0$ decreases and free Mg ion increases, the Mg/Ca ratio increases and dolomite is preferentially precipitated (Baker and Kastner, 1981). In semi-closed systems, such as burrows, and along the methane-rich fluid migration conduits and pathways, the sulphate consumption should reach maximum values; those should then be places of preferential dolomite precipitation. This process is interpreted to be dominant during the formation of the dolomite chimneys, that therefore record past fluid conduits where a steep-gradient SMTZ between the methane-rich environment of the conduit interior and the sulphate-rich porewaters around the fluid conduits (Fig. 7) was formed. Alternatively, dolomite precipitation can also occur as a result of more diffuse seepage regimes that result of a shallow SMTZ, or in areas of shallow SMTZ in between fluid migration conduits, most probably within the first meters of the sediment column, as suggested by the porewater profiles, which show Ca–Mg depletion, strongly associated with the methane and sulphate gradients (Hensen et al., 2007). This process can be responsible for the formation of the dolomite crusts along the SMTZ (Fig. 7). Biomarker and SEM observations indicate that microbial activity plays an important role in dolomite formation (Magalhães, 2007).

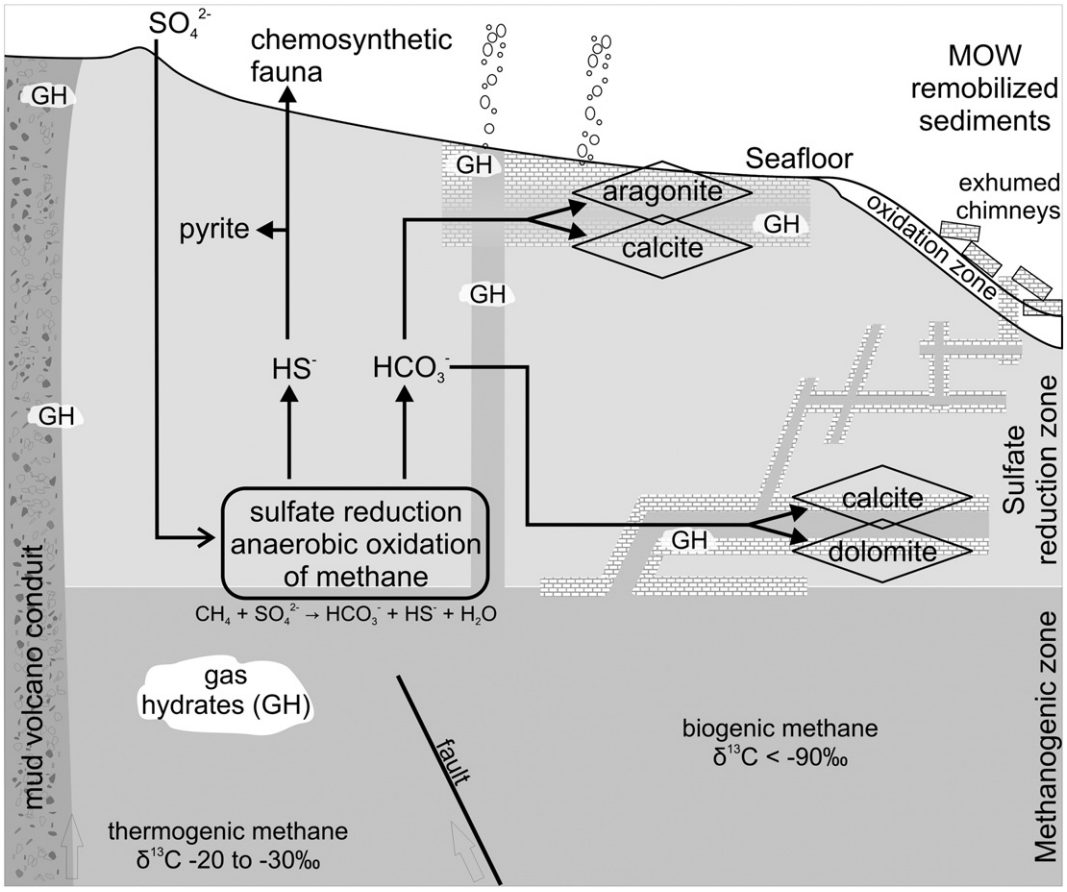

Fig. 7. Proposed schematic model for the formation of the methane-derived authigenic carbonates in the Gulf of Cadiz. The aragonite dominated carbonates are formed at or close to the seawater interface while the dolomite-dominated carbonates are formed within the sedimentary column along and around the fluid conduits.

5.2.2. Aragonite

Aragonite formation is favoured over calcite in seawater-ventilated environments, with high SO_4^{2-} concentrations and high Mg/Ca ratios (Burton, 1993), and at low phosphate and organic matter concentrations (Burton and Walter, 1990). As such, aragonite is preferentially formed in more open systems such as the sediment environments at or close to the seafloor. The precipitation of aragonite instead of calcite is favoured in seawater, as a result of the inhibiting effect of the hydrated Mg ions on the calcite structure. These environmental conditions are met when intense methane flux moves the SMTZ to very close to the seafloor. This is also supported by the petrographic characteristics of the aragonite dominated MDAC, that correspond to the cementation of sediments with high initial porosity and very low degrees of compaction.

5.3. Formation model of the different MDAC lithologies

5.3.1. Dolomite crusts, chimneys and irregular massive forms

Based on the underwater video observations, morphology, mineralogy, textural characteristics and geochemistry, a model for the formation of MDAC is proposed (Fig. 7). The dolomite crusts are interpreted as formed by cementation of subsurface permeable layers and the chimneys are interpreted as formed by cementation of subsurface sediments in and around fluid conduits (burrows, fractures and other sedimentary discontinuities). If the dolomite chimneys and crusts had formed above the seafloor they should contain a very small detrital fraction, limited to fine-grained hemipelagic sediments, and not a similar detrital composition and similar fabrics to those of the surrounding pelagic sediments, as observed (Fig. 5A,B). The low cement porosity also suggests that the cementation took place at a deeper level in the sediment column than the cementation of the aragonite-dominated carbonates. The occurrences of the dolomite chimneys and crusts are restricted to areas of strong bottom currents, mainly of the MOW. These bottom currents produce a subsequent erosion of the surrounding unconsolidated sediments, gradually exposing the dolomite chimneys and crusts. As they get exposed and lost support, they fell down on the seafloor, as observed by underwater video (Fig. 4A). The coatings of iron and manganese oxy-hydroxides, resulting from secondary oxidation of sulphur minerals (pyrite), as well as the colonisation by benthic fauna, begin after the chimneys are exposed at the seafloor. Dolomite chimneys with different oxidation intensities, different benthic fauna colonisation intensity, variable colour and variable thickness of the oxide coatings, reveal different periods of exposure to the seawater after exhumed. Depending on the sediment properties and fluid flow rate, different regimes of fluid flow can be imagined. *(1)* Regimes of diffuse fluid flow, which are expected to occur in sediments with larger grain size (sandy sediments), will not require open vent conduits. Dolomite chimneys with no vent channels will be produced under these regimes. *(2)* Fluid migration through clayish finer sediments, of low permeability, will preferentially be done through fractures, burrows, other sedimentary structures and heterogeneities, requiring open conduits or networks of conduits that, once opened, will be maintained open by the fluid flow (Stöhr et al., 2005). The authigenic cementation around these conduits will produce chimneys that will preserve the open vent channels. This is supported by the observation that chimneys with open vent channels are characterised by a finer (clay and silt) detrital fraction.

The large variability of shapes of the chimneys (helicoidal, parallel and branched) suggests a complex plumbing system of pathways for

fluid migration (Fig. 7). The helicoidal, curved and branched chimneys (Fig. 2F and 2G) probably correspond to cemented burrow infills, and are interpreted as pre-existing burrows that created preferential fluid flow pathways. Divergences of the fluid pathways will produce branched chimneys (Fig. 2G). The upward fluid migration, cutting sedimentary layers with variable permeability, resulting in different penetration of the fluid into the surrounding sediments and subsequent variable cementation, will develop chimneys with variable diameter (Fig. 2B–G) and/or irregular massive forms (Fig. 2H). In cases where the fluid migrates horizontally, along more permeable layers, slab-like crusts will be produced (Fig. 2A).

It is proposed that the ^{13}C-depleted methane fluids that migrate radially outward from the central vent conduits penetrate and mix with the surrounding porewaters, where sulphate reduction is active. Authigenic carbonates then precipitate radially from the vent conduit. This explains why the carbon isotope ratios of the dolomite become progressively heavier with increasing distance from the vent conduit. A similar explanation can be applied to the oxygen isotope ratios, assuming that the venting fluids have a contribution from ^{18}O-enriched porewaters resulting from gas hydrate dissociation (Magalhães, 2007). The degree of fluid penetration into the surrounding sediments is dependent on the initial permeability of the sediments, the fluid pressure, and the degree of cementation or rate of authigenic precipitation. The concentric rings observed in several chimneys, frequently each one with distinctive C and O isotopic compositions, can reflect individual episodes of venting, with different intensities and variable fluid compositions, or can reflect different mixing fronts between the methane-rich fluid and the surrounding porewater.

5.3.2. Aragonite crusts and pavements

The incorporation of *Calyptogena*, *Acharax*, open channels of Pogonophora and *Vestimentifera* casts, together with the high porosity of the aragonite pavements support the origin by near-surface cementation of existing soft sediments. Shell crusts therefore indicate in situ cementation of, most probably, live chemosynthetic communities. Seafloor observations (Fig. 4B–C) also support this as they show that active seep sites are characterised by rough surfaces with crusts and slabs, forming pavements and build-ups of cemented sediment. The mineral and geochemical characteristics of the aragonite pavements indicate formation under anoxic but seawater-ventilated environmental conditions (Fig. 7) as suggested for active seep sites e.g. at Hydrate Ridge (Greinert et al., 2001). This type of environment will be stabilised during times of high flux, when the SMTZ is moved up close to the seafloor (Fig. 7).

The extensive lithified mud volcano breccias are likely formed by an alternative mechanism, which does not involve active fluid venting over vast areas. After a mud volcano eruption, mud will be extruded producing flows that cover parts or all of the crater area, and eventually move down the mud volcano flanks as debris flows. This process produces reduced mixing of the bottom waters with the methane-rich, but sulphate and oxygen-depleted porewaters of the freshly emplaced mud breccias. After emplacement of the mud flow, methane oxidation will occur at the sediment–water interface and the oxidation front will progress downward according to the rates of methane flux due to compaction of the mud breccia and the downward diffusion of seawater dissolved SO_4^{2-} and O_2. This diffusion of SO_4^{2-} and O_2 is controlled not only by the chemical gradients but also by bioturbation and biological activity. The SMTZ is therefore located at or close to the seafloor and the subsequent precipitation of authigenic aragonite, calcite and Mg-calcite that lithifies the sediments resulting in the formation of the aragonite pavements. Both mechanisms of formation of the aragonite pavements: (i) high flux regimes that move the SMTZ close to the seafloor or (ii) emplacement of the methane rich mud volcano mud breccias, are compatible and may correspond to different time episodes of the evolution of a seep system.

The formation process of the intraformational breccias, characterised by fractures and pore spaces formed and maintained open during the cementation, is equivalent to the gas hydrate carbonates and aragonite collapse breccias described by Bohrmann et al. (1998) and Greinert et al. (2001). The brecciation that characterises these samples can result from ascending fluids, bubbles and pressure build-up, as a result of the accumulation of methane gas below the crust and subsequent violent gas escape, as described by Hovland et al. (1987) for MDAC in North Sea pockmarks. The growth of gas hydrate pieces or layers and subsequent decomposition produces volume expansion that can also disrupt the sediment at the seafloor and result in brecciation, as described for the shallow seeps on the Cascadia Subduction Zone's Hydrate Ridge (Bohrmann et al., 1998; Greinert et al., 2001, 2002) and in the Gulf of Mexico (MacDonald et al., 2003). As an alternative mechanism, gas hydrate formation of layers and veins, along which cementation by carbonates is hampered or prevented, is envisaged. While the host sediment that is free of hydrate is cemented, the hydrate-bearing parts will ultimately become pores after the gas hydrate decomposes (this can occur in situ or during sample recovery).

The stromatolitic layers observed are similar to those reported by Greinert et al. (2002) exhibiting inverted stromatolitic growth directions when compared with true stromatactis. Greinert et al. (2002) emphasised that the stromatolites in methane-derived crusts grow in the direction of the source of energy, protruding downward from shallow sediment horizons. AOM proceeds downward below pre-existing carbonate crusts and aggregates. The stromatolitic layers coat cavities and fractures, with botryoidal aragonite layers aggregating in the direction of the centre of the cavity. Frequently these cavities have lenticular shapes that resemble the shape of collected chunks of gas hydrates and are therefore interpreted as relicts of gas hydrate pieces or veins.

The presence of small amounts of dolomite in one aragonite pavement sample indicates that sulphate-depleted conditions that promote dolomite precipitation can be reached in a restricted environment, at a pore space scale, in the near-surface. Considering that dolomite formation is a process that is mediated by AOM-SR microbial consortia, this mediation preferentially induces the alteration of the microenvironment surrounding the bacteria cells (Vasconcelos et al., 2005), creating the optimal conditions for dolomite precipitation. The morphological and textural characteristics of the aragonite pavements show indications of recent or continuing formation, while the dolomite carbonates indicate an older formation.

6. Conclusions

MDAC from the Gulf of Cadiz occur as two main types: (I) dolomite crusts, irregular massive forms and chimneys, with the cement mineralogy dominated by dolomite and high-Mg calcite; and (II) aragonite pavements and build-ups, with cement mineralogy dominated by aragonite.

The different MDAC morphologies and different carbonate types reflect different methane-rich flow patterns through the sediments. If the flux is channelised through the SRZ of the sedimentary column, using burrows or sediment heterogeneities as pathways, an SMTZ and authigenic carbonate precipitation occurs around these fluid conduits. Because seawater circulation is limited in the conduits, sulphate depletion can be reached and dolomite will be the dominant mineralogy. The lithification of the sediments will result in the formation of the dolomite chimneys, crusts and irregular massive forms (Fig. 7). The locations where the dolomite chimneys have been recovered are presently swept by the flow of the Mediterranean undercurrent that can remobilize the unconsolidated sediments inside of which the chimneys here formed, and therefore produce the collapse of the individual chimneys, explaining their present horizontal position on the seafloor.

The aragonite pavements represent precipitation of authigenic carbonates in an environment closer to the seafloor interface. The aragonite pavements are formed at the sediment–seawater interface or close to it, resulting from an active and discrete venting or from a more diffuse and low-intensity venting process. Because these processes involve more direct interaction with seawater, where high alkalinity is coupled with high sulphate concentrations, the mineralogy is dominated by aragonite.

The MDAC are therefore interpreted as records of extensive methane seepage episodes in this particular area of the Gulf of Cadiz, spatially associated with probable deep-rooted fault systems, with mud volcanoes, mud diapirs and diapiric ridges, which constitute the preferential pathways for fluid migration. The oxygen isotopic composition and the mineralogy of the carbonates, for the assumed possible temperatures of formation, indicate that most of these carbonates precipitated in or near equilibrium with bottom-water conditions, but some carbonates with enriched ^{18}O indicate precipitation from ^{18}O-rich fluids, most probably derived from dissociation of gas hydrates. The MDAC also act as important reservoirs for carbon in the form of oxidised methane, in which microbial activity played a significant role.

Acknowledgements

This work and the ship time of Training-through-Research (TTR) cruises were funded jointly by the UNESCO/IOC, the University of Moscow, the *Laboratório Nacional de Energia e Geologia* (through the INGMAR Project—PLE/4/98, financed by the Portuguese Foundation for Science and Technology—FCT), the University of Aveiro (through the MVSEIS-Euromargins Project 01-LEC-EMA24F, financed by the FCT) and by the Spanish Foundation for Science and Technology (through the MVSEIS-Euromargins project REN2002-11669-E-MAR and CONSOLIDER-INGENIO 2010 CSD2006-0041-TOPOIBERIA). Special thanks to the TTRs and the TASYO/Anastasya crews and shipboard scientific parties. Many thanks to the Central Analysis Laboratory of the Aveiro University, in particular to S. Ribeiro for performing the Sr isotopic analyses used in this work. This work was developed as part of the Vitor Magalhães PhD project, supported by the FCT fellowship SFRH/BD/11747/2003. The authors thank the editor, Brian Jones, and two anonymous reviewers for their critical comments and suggestions that significantly improved the manuscript.

References

Aharon, P., Graber, E.R., Roberts, H.H., 1992. Dissolved carbon and delta-C-13 anomalies in the water column caused by hydrocarbon seeps on the northwestern Gulf of Mexico slope. Geo-Marine Letters 12 (1), 33–40.

Deep-water cold seeps, sedimentary environments and ecosystems of the Black and Tyrrhenian Seas and the Gulf of Cadiz. Preliminary results of investigations during the TTR-15 cruise of RV Professor Logachev June–August, 2005. In: Akhmetzhanov, A.M., Ivanov, M.K., Kenyon, N.H., Mazzini, A. (Eds.), IOC Technical Series, 72. United Nations Educational, Scientific and Cultural Organization, Paris. 140 pp.

Deep-water depositional systems and cold seeps of the Western Mediterranean, Gulf of Cadiz and Norwegian continental margins. In: Akhmetzhanov, A.M., Kenyon, N.H., Ivanov, M.K., Westbrook, G., Mazzini, A. (Eds.), Preliminary Results of Investigations during the TTR-16 Cruise of RV Professor Logachev May–July, 2006. Intergovernmental Oceanographic Commission technical series, 76. UNESCO, Paris. 91 pp.

Ambar, I., et al., 2002. Physical, chemical and sedimentological aspects of the Mediterranean outflow off Iberia. Deep Sea Research Part II: Topical Studies in Oceanography 49 (19), 4163–4177.

Baker, P.A., Kastner, M., 1981. Constrains on the formation of sedimentary dolomite. Science 213 (4504), 214–216.

Baringer, M.O.N., Price, J.F., 1999. A review of the physical oceanography of the Mediterranean outflow. Marine Geology 155 (1–2), 63–82.

Blinova, V., Ivanov, M., Pinheiro, L., 2006. Hydrocarbon gases and their possible source rock from mud volcanoes of the Gulf of Cadiz. In: Akhmanov, G.G. (Ed.), Geological Processes on Deep-water European Margins. International Conference and 15th Anniversary Training Through Research Post-Cruise Meeting, Moscow/Zvenigorod, Russia, pp. 10–11.

Boetius, A., et al., 2000. A marine microbial consortium apparently mediating anaerobic oxidation of methane. Nature 407 (6804), 623–626.

Bohm, F., et al., 2000. Oxygen isotope fractionation in marine aragonite of coralline sponges. Geochimica Et Cosmochimica Acta 64 (10), 1695–1703.

Bohrmann, G., Greinert, J., Suess, E., Torres, M., 1998. Authigenic carbonates from the Cascadia subduction zone and their relation to gas hydrate stability. Geology 26 (7), 647–650.

Bower, A.S., Serra, N., Ambar, I., 2002. Structure of the Mediterranean Undercurrent and Mediterranean Water spreading around the southwestern Iberian Peninsula. Journal of Geophysical Research 107 (C10), 3161. doi:10.1029/2001JC001007.

Buczynski, C., Chafetz, H.S., 1991. Habit of bacterially induced precipitates of calcium-carbonate and the influence of medium viscosity on mineralogy. Journal of Sedimentary Petrology 61 (2), 226–233.

Burton, E.A., 1993. Controls on marine carbonate cement mineralogy—review and reassessment. Chemical Geology 105 (1–3), 163–179.

Burton, E.A., Walter, L.M., 1990. The role of pH in phosphate inhibition of calcite and aragonite precipitation rates in seawater. Geochimica et Cosmochimica Acta 54 (3), 797–808.

Campbell, K.A., Farmer, J.D., Des Marais, D., 2002. Ancient hydrocarbon seeps from the Mesozoic convergent margin of California: carbonate geochemistry, fluids and palaeoenvironments. Geofluids 2 (2), 63–94.

Campbell, K.A., et al., 2010. Geological imprint of methane seepage on the seabed and biota of the convergent Hikurangi Margin, New Zealand: box core and grab carbonate results. Marine Geology 272 (1–4), 285–306.

Díaz-del-Río, V., et al., 2003. Vast fields of hydrocarbon-derived carbonate chimneys related to the accretionary wedge/olistostrome of the Gulf of Cádiz. Marine Geology 195 (1–4), 177–200.

Gardner, J.M., 2001. Mud volcanoes revealed and sampled on the Western Moroccan continental margin. Geophysical Research Letters 28 (2), 339–342.

Gardner, J.M., Jung, W., Somoza, L., 2001. The possible effect of the Mediterranean Outflow Water (MOW) on gas hydrate dissociation in the Gulf of Cadiz. 2001 AGU Fall Meeting. USA, San Francisco.

Gaspar, L.C., 1984. Geochemical characterization of phosphorites from the Portuguese Margin. Master Thesis, University of Aveiro, 81 pp.

Goldsmith, J.R., Graf, D.L., 1958. Relation between lattice constants and composition of the Ca–Mg carbonates. American Mineralogist 43 (1–2), 84–101.

Gonzalez, F.J., et al., 2009. Hydrocarbon-derived ferromanganese nodules in carbonate-mud mounds from the Gulf of Cadiz: mud-breccia sediments and clasts as nucleation sites. Marine Geology 261 (1–4), 64–81.

Gournay, J.P., Kirkland, B.L., Folk, R.L., Lynch, F.L., 1999. Nanometer-scale features in dolomite from Pennsylvanian rocks, Paradox Basin, Utah. Sedimentary Geology 126 (1–4), 243–252.

Greinert, J., Bohrmann, G., Suess, E., 2001. Gas hydrate-associated carbonates and methane-venting at Hydrate Ridge: classification, distribution, and origin of authigenic lithologies. In: Paull, C.K., Dillon, W.P. (Eds.), Natural Gas Hydrates: Occurrence, Distribution, and Detection. Geophysical Monograph Series. American Geophysical Union, Washington, pp. 99–113.

Greinert, J., Bohrmann, G., Elvert, M., 2002. Stromatolitic fabric of authigenic carbonate crusts: result of anaerobic methane oxidation at cold seeps in 4,850 m water depth. International Journal of Earth Sciences 91, 698–711.

Gutscher, M.-A., et al., 2002. Evidence for active subduction beneath Gibraltar. Geology 30 (12), 1071–1074.

Hensen, C., et al., 2007. Sources of mud volcano fluids in the Gulf of Cadiz—indications for hydrothermally altered fluids. Geochimica et Cosmochimica Acta 71 (5), 1232–1248. doi:10.1016/j.gca.2006.11.022.

Hernandez-Molina, F.J., et al., 2006. The contourite depositional system of the Gulf of Cadiz: a sedimentary model related to the bottom current activity of the Mediterranean Outflow Water and its interaction with the continental margin. Deep Sea Research Part II: Topical Studies in Oceanography 53 (11–13), 1420–1463.

Hovland, M., Talbot, M.R., Qvale, H., Olaussen, S., Aasberg, L., 1987. Methane-related carbonate cements in pockmarks of the North-Sea. Journal of Sedimentary Petrology 57 (5), 881–892.

Judd, A., Hovland, M., 2007. Seabed Fluid Flow. The Impact on Geology, Biology and the Marine Environment. Cambridge University Press, Cambridge, New York, Melbourne, Madrid, Cape Town, Singapore, Sao Paulo. 475 pp.

Multidisciplinary study of geological processes on the north east Atlantic and western Mediterranean Sea margins. In: Kenyon, N.H., Ivanov, M.K., Akhmetzhanov, A.M., Akhmanov, G.G. (Eds.), Preliminary Results of Geological and Geophysical Investigations during the TTR-9 Cruise of R/V Professor Logachev June–July, 1999. Intergovernmental Oceanographic Commission (IOC) technical series, 56. UNESCO, Paris. 102 pp.

Interdisciplinary approaches to geoscience on the north east Atlantic margin and Mid-Atlantic Ridge. In: Kenyon, N.H., Ivanov, M.K., Akhmetzhanov, A.M., Akhmanov, G.G. (Eds.), Preliminary Results of Investigations during the TTR-10 Cruise of RV Professor Logachev. July–August, 2000. Intergovernmental Oceanographic Commission (IOC) technical series, 60. UNESCO, Paris. 104 pp.

Geological processes in the Mediterranean and Black Seas and north east Atlantic. In: Kenyon, N.H., Ivanov, M.K., Akhmetzhanov, A.M., Akhmanov, G.G. (Eds.), Preliminary Results of Investigations during the TTR-11 Cruise of RV Professor Logachev July–September, 2001. IOC Technical Series, 62. United Nations Educational, Scientific and Cultural Organization, Paris. 89 pp.

Interdisciplinary geoscience research on the north east Atlantic margin, Mediterranean Sea and Mid-Atlantic Ridge. In: Kenyon, N.H., Ivanov, M.K., Akhmetzhanov, A.M., Akhmanov, G.G. (Eds.), Preliminary Results of Investigations during the TTR-12 Cruise of RV Professor Logachev June–August, 2002. IOC Technical Series, 67. United Nations Educational, Scientific and Cultural Organization, Paris. 112 pp.

Interdisciplinary geoscience studies of the Gulf of Cadiz and Western Mediterranean basins. In: Kenyon, N.H., Ivanov, M.K., Akhmetzhanov, A.M., Akhmanov, G.G.

(Eds.), Preliminary Results of Investigations during the TTR-14 Cruise of RV Professor Logachev July–September, 2004. IOC Technical Series, 70. United Nations Educational, Scientific and Cultural Organization, Paris. 115 pp.
Kim, S.-T., O'Neil, J.R., 1997. Equilibrium and nonequilibrium oxygen isotope effects in synthetic carbonates. Geochimica et Cosmochimica Acta 61 (16), 3461–3475.
Kinnaman, F.S., Valentine, D.L., Tyler, S.C., 2007. Carbon and hydrogen isotope fractionation associated with the aerobic microbial oxidation of methane, ethane, propane and butane. Geochimica et Cosmochimica Acta 71 (2), 271–283.
Kopf, A., et al., 2004. Report and Preliminary Results of Sonne Cruise SO175, p. 228. Bremen.
Kulm, L.D., Suess, E., 1990. Relationship between carbonate deposits and fluid venting: Oregon accretionary prism. Journal of Geophysical Research-Solid Earth and Planets 95 (B6), 8899–8915.
Kulm, L.D., et al., 1986. Oregon subduction zone: venting, fauna, and carbonates. Science 231 (4738), 561–566.
León, R., et al., 2006. Classification of sea-floor features associated with methane seeps along the Gulf of Cádiz continental margin. Deep Sea Research Part II: Topical Studies in Oceanography 53 (11–13), 1464–1481.
León, R., et al., 2010. Pockmarks, collapses and blind valleys in the Gulf of Cádiz. Geo-Marine Letters 30 (3–4), 231–247.
Lumsden, D.N., 1979. Discrepancy between thin-section and X-ray estimates of dolomite in limestone. Journal of Sedimentary Petrology 49, 429–435.
MacDonald, I.R., Sager, W.W., Peccini, M.B., 2003. Gas hydrate and chemosynthetic biota in mounded bathymetry at mid-slope hydrocarbon seeps: Northern Gulf of Mexico. Marine Geology 198 (1–2), 133–158.
Magalhães, V.H., 2007. Authigenic carbonates and fluid escape structures in the Gulf of Cadiz. Doctoral Thesis, University of Aveiro, Aveiro, 421 pp.
Martin-Puertas, C., et al., 2007. A comparative mineralogical study of gas-related sediments of the Gulf of Cadiz. Geo-Marine Letters 27 (2–4), 223–235. doi:10.1007/s00367-007-0075-1.
Matsumoto, R., 1990. Vuggy carbonate crust formed by hydrocarbon seepage on the continental shelf of Baffin Island, northeast Canada. Geochemical Journal 24 (3), 143–158.
Mazurenko, L.L., Soloviev, V.A., Belenkaya, I., Ivanov, M.K., Pinheiro, L.M., 2002. Mud volcano gas hydrates in the Gulf of Cadiz. Terra Nova 14 (5), 321–329.
Medialdea, T., et al., 2004. Structure and evolution of the "Olistostrome" complex of the Gibraltar Arc in the Gulf of Cadiz (eastern Central Atlantic): evidence from two long seismic cross-sections. Marine Geology 209 (1–4), 173–198.
Medialdea, T., et al., 2009. Tectonics and mud volcano development in the Gulf of Cadiz. Marine Geology 261 (1–4), 48–63.
Meister, P., McKenzie, J.A., Warthmann, R., Vasconcelos, C., 2006. Mineralogy and petrography of Diagenetic Dolomite from the ODP Leg 201 Peru margin drill sites. Proc. ODP, Sci. Results.
Meister, P., et al., 2007. Dolomite formation in the dynamic deep biosphere: results from the Peru Margin (ODP Leg 201). Sedimentology 54 (5), 1007–1032.
Moore, T.S., Murray, R.W., Kurtz, A.C., Schrag, D.P., 2004. Anaerobic methane oxidation and the formation of dolomite. Earth and Planetary Science Letters 229 (1–2), 141–154.
Morse, J.W., Wang, Q.W., Tsio, M.Y., 1997. Influences of temperature and Mg:Ca ratio on $CaCO_3$ precipitates from seawater. Geology 25 (1), 85–87.
Niemann, H., et al., 2006. Microbial methane turnover at mud volcanoes of the Gulf of Cadiz. Geochimica et Cosmochimica Acta 70 (21), 5336–5355.
Nuzzo, M., et al., 2009. Origin of light volatile hydrocarbon gases in mud volcano fluids, Gulf of Cadiz—evidence for multiple sources and transport mechanisms in active sedimentary wedges. Chemical Geology 266 (3–4), 350–363.
Nyman, S.L., Nelson, C.S., Campbell, K.A., 2010. Miocene tubular concretions in East Coast Basin, New Zealand: analogue for the subsurface plumbing of cold seeps. Marine Geology 272 (1–4), 319–336.
Olu-Le Roy, K., et al., 2004. Cold seep communities in the deep eastern Mediterranean Sea: composition, symbiosis and spatial distribution on mud volcanoes. Deep Sea Research Part I: Oceanographic Research Papers 51 (12), 1915–1936.
Orpin, A.R., 1997. Dolomite chimneys as possible evidence of coastal fluid expulsion, uppermost Otago continental slope, southern New Zealand. Marine Geology 138 (1–2), 51–67.
Paull, C.K., Jull, A.J.T., Toolin, L.J., Linick, T., 1985. Stable isotope evidence for chemosynthesis in an abyssal seep community. Nature 317 (6039), 709–711.
Paull, C.K., et al., 1992. Indicators of methane-derived carbonates and chemosynthetic organic carbon deposits: examples from the Florida Escarpment. Palaios 7, 361–375.
Paytan, A., Kastner, M., Martin, E.E., Macdougall, J.D., Herbert, T., 1993. Marine barite as a monitor of seawater Strontium isotope composition. Nature 366 (6454), 445–449.
Peckmann, J., Thiel, V., 2004. Carbon cycling at ancient methane-seeps. Chemical Geology 205 (3–4), 443–467.
Peckmann, J., et al., 2001. Methane-derived carbonates and authigenic pyrite from the northwestern Black Sea. Marine Geology 177 (1–2), 129–150.
Pinheiro, L.M., et al., 2003. Mud volcanism in the Gulf of Cadiz: results from the TTR-10 cruise. Marine Geology 195 (1–4), 131–151.
Pinheiro, L.M., et al., 2006. Structural control of mud volcanism and hydrocarbon-rich fluid seepage in the gulf of Cadiz: recent results from the TTR-15 cruise. In: Mascle, J., Sakellariou, D., Briand, F. (Eds.), Fluid Seepages/Mud Volcanism in the Mediterranean and Adjacent Domains: CIESM Workshop Monographs, n°29, pp. 53–58. Bologna, Italy.
Reeburgh, W.S., 1980. Anaerobic methane oxidation: rate depth distributions in Skan Bay sediments. Earth and Planetary Science Letters 47, 345–352.
Reitner, J., et al., 1995. Mud mounds: a polygenetic spectrum of fine-grained carbonate buildups. Facies 32, 1–69.
Ritger, S., Carson, B., Suess, E., 1987. Methane-derived authigenic carbonates formed by subduction-induced pore-water expulsion along the Oregon/Washington margin. Geological Society of America Bulletin 98 (2), 147–156.
Roberts, H.H., Aharon, P., 1994. Hydrocarbon-derived carbonate buildups of the northern Gulf of Mexico continental slope: a review of submersible investigations. Geo-Marine Letters 14 (2–3), 135–148.
Rodrigues, C.F., Cunha, M., 2005. Common chemosynthetic species in the Gulf of Cadiz: some data on their spatial distribution. In: Hamoumi, N., Henriet, J.P., Kenyon, N., Suzyumov, A.E. (Eds.), Geosphere–Biosphere Coupling Processes: The TTR Interdisciplinary Approach towards Studies of the European and North African margins International Conference and Post-Cruise Meeting of the Training-Through-Research Programme. : Workshop Report. UNESCO/IOC, Marrakech, Morocco, pp. 26–28.
Rosenbaum, J., Sheppard, S.M.F., 1986. An isotopic study of siderites, dolomites and ankerites at high-temperatures. Geochimica et Cosmochimica Acta 50 (6), 1147–1150.
Schonfeld, J., 2001. Benthic foraminifera and pore-water oxygen profiles: a re-assessment of species boundary conditions at the western Iberian Margin. Journal of Foraminiferal Research 31 (2), 86–107.
Sibuet, M., Olu, K., 1998. Biogeography, biodiversity and fluid dependence of deep-sea cold-seep communities at active and passive margins. Deep Sea Research Part II 45 (1–3), 517–567.
Somoza, L., et al., 2002. Numerous methane gas-related sea floor structures identified in Gulf of Cadiz. Eos 83 (47), 541–549.
Somoza, L., et al., 2003. Seabed morphology and hydrocarbon seepage in the Gulf of Cádiz mud volcano area: acoustic imagery, multibeam and ultra-high resolution seismic data. Marine Geology 195 (1–4), 153–176.
Stadnitskaia, A., et al., 2001. Molecular and isotopic characterization of hydrocarbon gas and organic matter from mud volcanoes of the Gulf of Cadiz, NE Atlantic. International Conference and 10th Anniversary Training Through Research Post-Cruise Meeting, Moscow/Mozhenka, Russia, pp. 90–91.
Stadnitskaia, A., Ivanov, M.K., Blinova, V., Kreulen, R., van Weering, T.C.E., 2006. Molecular and carbon isotopic variability of hydrocarbon gases from mud volcanoes in the Gulf of Cadiz, NE Atlantic. Marine and Petroleum Geology 23 (3), 281–296.
Stöhr, M., Boetius, A., Khalili, A., 2005. Flow and transport in permeable sediments induced by gas seepage. European Geosciences Union 2005. : Geophysical Research Abstracts. European Geosciences Union, Vienna, Austria, p. 07548.
Terrinha, P., et al., 2009. Morphotectonics and Strain Partitioning at the Iberia–Africa plate boundary from multibeam and seismic reflection data. Marine Geology 267, 156–174.
Van Lith, Y., Warthmann, R., Vasconcelos, C., McKenzie, J.A., 2003. Microbial fossilization in carbonate sediments: a result of the bacterial surface involvement in dolomite precipitation. Sedimentology 50 (2), 237–245.
Vasconcelos, C., McKenzie, J.A., Bernasconi, S., Grujic, D., Tien, A.J., 1995. Microbial mediation as a possible mechanism for natural dolomite formation at low temperatures. Nature 377, 220–222.
Vasconcelos, C., McKenzie, J.A., Warthmann, R., Bernasconi, S.M., 2005. Calibration of the $\delta^{18}O$ paleothermometer for dolomite precipitated in microbial cultures and natural environments. Geology 33 (4), 317–320.
Voelker, A.H.L., et al., 2006. Mediterranean outflow strengthening during northern hemisphere coolings: a salt source for the glacial Atlantic? Earth and Planetary Science Letters 245 (1–2), 39–55.
Wiedicke, M., Weiss, W., 2006. Stable carbon isotope records of carbonates tracing fossil seep activity off Indonesia. Geochemistry, Geophysics, Geosystems 7, Q11009. doi:10.1029/2006GC001292.